

Journal of Biomedical Optics

SPIEDigitalLibrary.org/jbo

Fluorescence background subtraction technique for hybrid fluorescence molecular tomography/x-ray computed tomography imaging of a mouse model of early stage lung cancer

Angelique Ale
Vladimir Ermolayev
Nikolaos C. Deliolanis
Vasilis Ntziachristos

Fluorescence background subtraction technique for hybrid fluorescence molecular tomography/x-ray computed tomography imaging of a mouse model of early stage lung cancer

Angelique Ale,^{a,b} Vladimir Ermolayev,^a Nikolaos C. Deliolanis,^{a,c} and Vasilis Ntziachristos^a

^aTechnische Universität München and Helmholtz Zentrum München, Institute for Biological and Medical Imaging, Ingolstädter Landstrasse 1, D-85764 Neuherberg, Germany

^bImperial College London, Division of Molecular Biosciences, Theoretical Systems Biology Group, London SW7 2AZ, United Kingdom

^cFraunhofer Project Group for Automation in Medicine and Biotechnology, Theodor-Kutzer-Ufer 1-3, 68167, Mannheim, Germany

Abstract. The ability to visualize early stage lung cancer is important in the study of biomarkers and targeting agents that could lead to earlier diagnosis. The recent development of hybrid free-space 360-deg fluorescence molecular tomography (FMT) and x-ray computed tomography (XCT) imaging yields a superior optical imaging modality for three-dimensional small animal fluorescence imaging over stand-alone optical systems. Imaging accuracy was improved by using XCT information in the fluorescence reconstruction method. Despite this progress, the detection sensitivity of targeted fluorescence agents remains limited by nonspecific background accumulation of the fluorochrome employed, which complicates early detection of murine cancers. Therefore we examine whether x-ray CT information and bulk fluorescence detection can be combined to increase detection sensitivity. Correspondingly, we research the performance of a data-driven fluorescence background estimator employed for subtraction of background fluorescence from acquisition data. Using mice containing known fluorochromes *ex vivo*, we demonstrate the reduction of background signals from reconstructed images and sensitivity improvements. Finally, by applying the method to *in vivo* data from K-ras transgenic mice developing lung cancer, we find small tumors at an early stage compared with reconstructions performed using raw data. We conclude with the benefits of employing fluorescence subtraction in hybrid FMT-XCT for early detection studies. © 2013 Society of Photo-Optical Instrumentation Engineers (SPIE)

[DOI: [10.1117/1.JBO.18.5.056006](https://doi.org/10.1117/1.JBO.18.5.056006)]

Keywords: fluorescence tomography; image reconstruction; multimodality; targeted fluorescence agent.

Paper 130002R received Jan. 2, 2013; revised manuscript received Mar. 26, 2013; accepted for publication Mar. 26, 2013; published online May 2, 2013.

1 Introduction

Fluorescence molecular tomography (FMT) is a noninvasive optical imaging method aimed at monitoring fluorescence bio-distribution in small-animals *in vivo*.^{1,2} In FMT, typically a fluorescent agent is injected into a mouse, and focused light is subsequently scanned across the animal surface, after which excitation and fluorescence photons that have propagated through the tissue are collected. The acquired data is combined in a mathematical inversion scheme to produce quantitative images of fluorescence bio-distribution. Over the past years, the technique has evolved from limited-angle trans-illumination geometries to charge coupled device (CCD) camera-based 360-deg trans-illumination systems, enabling FMT to deliver molecular contrast with millimeter resolution.³ A significant challenge in optical imaging is the highly diffusive nature of photons propagating in tissue.^{4,5} Furthermore, while FMT delivers molecular contrast, the modality does not provide anatomical information. To address these challenges, recent technical and performance advances have focused on the combination of FMT with modalities that offer anatomical information

including magnetic resonance imaging and x-ray computed tomography (XCT).⁶⁻⁹ The use of anatomical data can improve optical tomography by building geometrically accurate forward photon propagation models in the tissue imaged.¹⁰⁻¹² Second, the anatomical information has been employed to reduce the uncertainty of the ill-posed FMT inverse problem by using anatomical information as image priors.^{10,13} In post-processing the FMT data, the anatomical information is used to provide the anatomical context for the reconstructed fluorescence signals. The improved imaging capabilities have been recently demonstrated in complex areas of the mouse, such as the thorax area, for example, and imaging bone disease or lung cancer in animal models.¹³ Detection of lung tumors with fluorescence tomography has also been reported using limited-projection FMT¹⁴ and early photon FMT.¹⁵ An important next step toward improved image quality is to include the newly available anatomical information in the preprocessing of the FMT data before reconstruction of the fluorescence signal, by using it to apply a background fluorescence correction, which will be described in this paper.

Background fluorescence can be largely attributed to nonspecific distribution or binding of the fluorescence agents employed for imaging, which are typically administered intravenously.

Address all correspondence to: Vasilis Ntziachristos, Technische Universität München & Helmholtz Zentrum München, Institute for Biological and Medical Imaging, Ingolstädter Landstrasse 1, D-85764 Neuherberg, Germany. Tel: +49-89-3187-3852; Fax: +49-89-3187-3017; E-mail: v.ntziachristos@tum.de

After circulation through the body, the fluorescent agent typically accumulates at the target site (for example, a tumor), resulting in a larger concentration of probe at the specific site. However, the presence of the agent throughout the body, even at low concentrations, suffices to generate signals that can be detected and contribute to reducing the contrast in the image or even masking small target lesions. Background fluorescence contributions may also be due to the auto-fluorescence of tissue and fluorochromes present in the mouse diet, but these contributions are typically minor in the near-infrared, unless the skin or the gastro-intestinal system are imaged.^{16–18}

Reduction of background fluorescence in the tissue is especially important when the aim is to visualize small targets with a low-fluorescence intensity. This situation occurs particularly when imaging lung tumor development at an early stage. Early stage imaging can allow identification of biomarkers involved in disease development and progression. However, the imaging of small and nonbright tumors that characterize early stage lung cancer can be obstructed by the presence of background fluorescence in the tissue.

Methods for reducing the influence of background fluorescence on the reconstruction result have been previously investigated.^{18–24} One approach constrained the inversion step of the reconstruction of the fluorescence distribution in the presence of background fluorescence. The maximum level of background fluorescence was calculated by taking the ratio of the measurements at the detectors divided by the corresponding weight matrix integrated over the complete volume. This maximum level was used to set a lower bound for the reconstructed fluorescence concentration.¹⁹ Several multispectral approaches for reducing the effects of background fluorescence have been investigated.^{20,22,23} Deliolanis et al.²⁰ performed additional multispectral measurements using shorter wavelengths, which were subtracted from the measurements obtained by excitation at the peak excitation wavelength of the probe. Tichauer et al.²³ recently developed a method that involves subtraction of the signal of a second, untargeted fluorescent tracer with similar characteristics as the targeted tracer. Preprocessing of the measured data has also been considered, before using them as input for the inversion.^{18,21} Gao et al.¹⁸ plotted the normalized Born ratio as a function of the two-dimensional (2-D) radial distance from the source point projected on the CCD camera plane. A cubic polynomial was fitted to the lower bound of the plot, and subsequently this polynomial was subtracted from the normalized Born ratios. Soubret et al.²¹ proposed a subtraction method for a slab geometry, under the assumption that the background fluorescence and the tissue/object imaged were both homogeneous. This method observed a linear relationship between the tissue background fluorescence and the normalized Born values measured, as a function of the distance between the source and the detector involved in each measurement. A proportionality constant was then calculated and applied as a data preprocessing step to demonstrate imaging improvements. Although the assumption of a slab geometry is appropriate when using an imaging chamber, it remains an approximation. The latest developments of FMT systems are generally free-space implementations, for which the assumption of a slab geometry is less appropriate. Furthermore, it has been shown recently that also in systems where the mouse is imaged in a cassette, reconstruction of the fluorescence distribution is significantly improved by including accurate anatomical information.²⁵ The same is expected when incorporating

anatomical information for performing a background fluorescence subtraction.

In this paper, we interrogate whether the fluorescence subtraction scheme developed in Ref. 21 for slab geometry can be applied to 360-deg acquisition geometry, as it relates to imaging with a hybrid FMT-XCT system. A major advantage of hybrid FMT-XCT is that both modalities are implemented in the same system, which minimizes the time difference between acquisition of FMT and XCT data and eliminates the need to move the animal in between scans, resulting in an accurate match of data from both modalities, which was not previously available. We describe the steps of implementing the background fluorescence subtraction method for 360-deg geometries and employing XCT information. Most important, we implemented it in a data-driven way. We demonstrate our findings on imaging performance and quantification using *ex vivo* mouse measurements, as well as *in vivo* studies employing transgenic mice developing spontaneous lung tumors.²⁶

2 Methods

2.1 Expression for Normalized Background Fluorescence

The normalized Born approximation is a data-conditioning method employed in fluorescence tomography to minimize the sensitivity of the reconstruction on experimental uncertainties, in particular the unknown gain and attenuation factors involved in tomographic measurements (gain of each detector employed, strength of each source, etc.). A further benefit of this normalization is the reduced sensitivity of the reconstruction to spatial variations in absorption properties within tissues, whereby scattering variations remain challenging.¹² According to the normalized Born method, the emission measurements at the wavelength of the fluorochrome $U^{\text{fl}}(\vec{r}_d, \vec{r}_s)$ are normalized by the measured transmittance $U^{\text{exc}}(\vec{r}_d, \vec{r}_s)$ at the excitation wavelength of the laser:

$$[U^{\text{NB}}(\vec{r}_d, \vec{r}_s)]_{\text{measured}} = \frac{U^{\text{fl}}(\vec{r}_d, \vec{r}_s)}{U^{\text{exc}}(\vec{r}_d, \vec{r}_s)}, \quad (1)$$

where $[U^{\text{NB}}(\vec{r}_d, \vec{r}_s)]_{\text{measured}}$ represents the normalized measurements corresponding with a source at \vec{r}_s and a virtual detector at \vec{r}_d . For the case of a homogeneous medium with a constant fluorescence level throughout the medium, Soubret and Ntziachristos²¹ derived a linear relationship between the Born ratio and the distance from source to detector, given by

$$U_{\text{target}}^{\text{NB}}(\vec{r}_d, \vec{r}_s) = [U^{\text{NB}}(\vec{r}_d, \vec{r}_s)]_{\text{measured}} - a \|\vec{r}_d - \vec{r}_s\|, \quad (2)$$

where $\|\vec{r}_d - \vec{r}_s\|$ is the distance from a source at \vec{r}_s to a detector at \vec{r}_d , a is a constant proportional to the constant fluorescence level in the medium, and $U_{\text{target}}^{\text{NB}}(\vec{r}_d, \vec{r}_s)$ is the data corrected for background fluorescence. The parameters that need to be estimated to obtain $U_{\text{target}}^{\text{NB}}(\vec{r}_d, \vec{r}_s)$ are the proportionality constant a and the distance from source to detector $\|\vec{r}_d - \vec{r}_s\|$.

2.2 Calculation of Distances

In this work, we explored whether the relationship in Eq. (2) is applicable to measurements collected over 360 deg as available by hybrid FMT-XCT systems. XCT anatomical information was employed to calculate the distance between source and detector

FMT pairs, as they are established in a noncontact manner on the mouse surface.

For each CCD viewing angle, the points on the mouse surface seen by the camera were extracted from the cross-section of the XCT derived surface and lines perpendicular to the CCD detection plane, forming the three-dimensional (3-D) surface of the imaged medium at the side of the CCD plane, S_{CCD} . In the same way, all points on the mouse surface as seen by a virtual camera at the source plane were extracted, forming the 3-D surface of the medium at the side of the source plane S_{source} [Fig. 1(a)].

The extracted surface S_{CCD} was interpolated on a grid of 512×512 points corresponding to the pixels in the CCD camera image, resulting in a 512×512 image. The 3-D Euclidian distance from the source point \vec{r}_s projected at the source surface S_{source} to all points on the interpolated surface image at the detector side S_{CCD} was calculated. This resulted in a 512×512 image of distances, IM_{BG} [Fig. 1(b)], representing the term $\|\vec{r}_d - \vec{r}_s\|$, for each pixel in a corresponding acquisition image IM_{acq} [Fig. 1(e)] obtained by measurement with the hybrid FMT-XCT system.

2.3 Data-Driven Proportionality Estimation

The next step was to derive a method that automatically calculates a proportionality factor a as per Eq. (2), for each mouse studied. To perform this calculation, all measurements in an acquired data set obtained from a mouse scan were considered. In a typical FMT-XCT imaging protocol data from 18 angular projections are acquired. For each projection, a total of 18 sources were scanned resulting in a total data volume of 324 images per wavelength. Then a region of interest was automatically selected on a per-image basis as the area that was covered by the scanned sources. This area was employed for the calculation of the proportionality factor. This calculation assumes that there is an underlying fluorescence background

distribution that is present in all measurements (scaled with distance). In case the medium would contain background fluorescence only, i.e., $U_{\text{target}}^{\text{NB}}(\vec{r}_d, \vec{r}_s)$ is zero in Eq. (2), an estimate of the proportionality constant a calculated for one source detector pair $\hat{a}(\vec{r}_d, \vec{r}_s)$ would be given by

$$\hat{a}(\vec{r}_d, \vec{r}_s) = \frac{[U^{\text{NB}}(\vec{r}_d, \vec{r}_s)]_{\text{measured}}}{\|\vec{r}_d - \vec{r}_s\|}, \quad (3)$$

where $\hat{a}(\vec{r}_d, \vec{r}_s)$ is a constant proportional to the background fluorescence level, $\|\vec{r}_d - \vec{r}_s\|$ is the distance from a source at \vec{r}_s to a detector at \vec{r}_d , and $[U^{\text{NB}}(\vec{r}_d, \vec{r}_s)]_{\text{measured}}$ represents the normalized measurements corresponding to a source at \vec{r}_s and a detector at \vec{r}_d . To estimate one proportionality factor a on a per mouse basis, we assumed that the mice scanned contained only background fluorescence. Generally, this assumption is approximately true if the fluorescent target tissue volume for an injected fluorochrome is smaller than the total mouse volume visualized, which is typically the case when imaging tumors or specific organ parts. Using Eq. (3), the $\hat{a}(\vec{r}_d, \vec{r}_s)$ for each source detector pair was calculated, and the distribution of the $\hat{a}(\vec{r}_d, \vec{r}_s)$ values for all source-detector pairs ($\sim 10^7$) was plotted. With the assumption then that the fluorescent source is small compared with the total mouse volume scanned, the most frequent value observed (the mode) was used as the estimate of the proportionality constant a on a per-mouse basis:

$$a = \text{bin}(\max\{\text{hist}[\hat{a}(\vec{r}_d, \vec{r}_s)]\}), \quad (4)$$

thus providing a robust and fully data driven method to determine a . In Fig. 1(c), the distribution of the ratio of the pixels in the region of interest of IM_{BG} [Fig. 1(b)] divided by IM_{acq} [Fig. 1(e)], a can be found at the peak value, in this case a is approximately 0.2. The last step in the background correction was the subtraction of the background images IM_{BG} from the

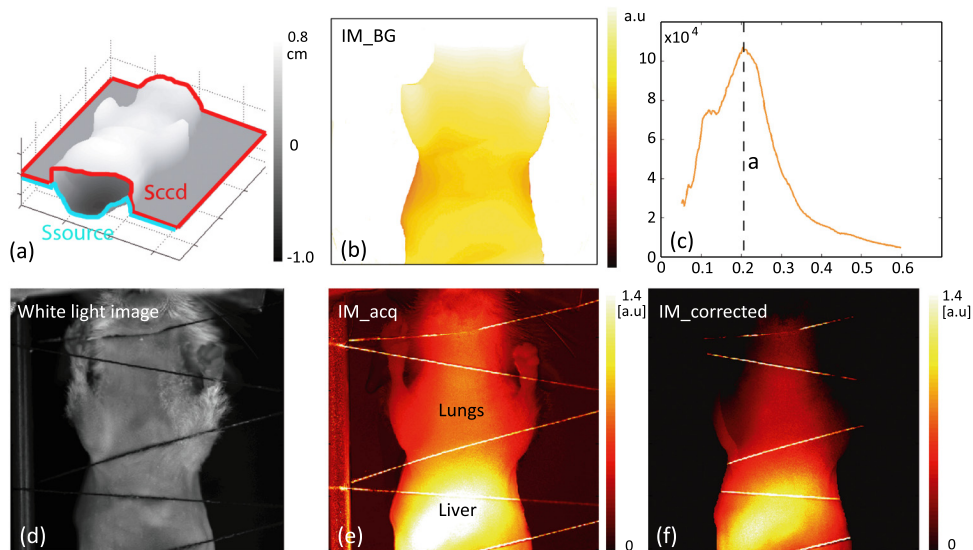


Fig. 1 Steps in the calculation of the background fluorescence corrected data set: (a) example of calculated surfaces at the side of source S_{source} and camera S_{CCD} for one gantry angle (205 deg), units in cm corresponding with distance from the indicated plane; (b) calculated background fluorescence image, IM_{BG} for one source based on the 3-D distances from source point on source surface to camera surface; (c) histogram of background fluorescence/acquisition image per pixel in a region of interest on the mouse surface, estimated value of a is indicated by the dotted line; (d) white light image of the mouse (ventral side); (e) normalized acquisition data, IM_{acq} ; and (f) background corrected data, $\text{IM}_{\text{corrected}}$.

acquisition data IM_{acq} using the proportionality factor a and Eq. (2):

$$IM_{corrected} = IM_{acq} - a \cdot IM_{BG}. \quad (5)$$

The corrected acquisition images $IM_{corrected}$ are used as input for the reconstruction of the fluorescence distribution, i.e., the operation is performed on the acquisition images directly, before source-detector pairs are extracted from the images for reconstruction.

2.4 Hybrid FMT-XCT Imaging and Reconstruction

The system that was used for hybrid FMT-XCT imaging was described in detail in Ref. 6. It was a hybrid combination of a gantry based micro-CT system (eXplore Locus, GE HealthCare, Ontario, Canada) and free-space FMT instrumentation in trans-illumination setup. The rotating gantry enabled FMT and XCT acquisition over the full 360-deg range, resulting in a hybrid FMT-XCT data set.

The 3-D fluorescence distribution was reconstructed from the acquisition data using a “double prior” hybrid reconstruction method, described in detail in Ref. 13. This method combines a finite element method (FEM) based optical forward model that employs XCT information to allocate organ-specific optical properties with a selfregularized inversion scheme also based on XCT priors. For the background correction, the background fluorescence was subtracted from the data and then used as an input for the reconstruction as in Ref. 13.

2.5 Animal Studies

Ex vivo animal studies were performed to evaluate the performance of the method using controlled tissue measurements. For this purpose, a euthanized nude mouse was employed, and a 1-mm diameter translucent tube was inserted in the esophagus until it reached the upper stomach. The translucent tube was filled with three mixtures containing intralipid, India ink, water, and 670/710-nm excitation/emission fluorochrome at three concentrations (1) control (0), (2) 1.4 μ M, and (3) at 11 μ M.

In vivo animal studies were also performed to investigate the performance of the method in living tissues. We were particularly interested in studying small tumors, early in their development and interrogated whether detection improvements could be afforded using fluorescence subtraction. For this reason, we employed a K-ras mouse model bearing mutated human K-ras^{G12D} allele, which develops lung cancer with high incidence upon spontaneous recombination events.²⁶ We created double transgenic K-ras +/– and BL6 Tyr –/– mice, derived from mouse lines purchased from the Jackson Laboratory, Maine, USA, and crossed in our laboratory. This double transgenic mouse line is white and develops lung tumors similar to a parent K-ras +/– line. 2 nmol of a probe targeting $\alpha v\beta 3$ (IntegriSense 680, excitation: 680 nm, emission: 710 nm, Perkin Elmer) was injected 24 h prior to imaging. We imaged four-week-old mice. All animal experiments were approved by the government of Bavaria and conformed to rules and regulations of Helmholtz Zentrum München.

2.6 Validation Methods

Animals imaged *in vivo* by FMT-XCT were euthanized by an intra-peritoneal Ketamin and Xylazine injection and were embedded in an optimal cutting temperature (OCT) compound mixed with black India ink and frozen to -80°C . For validation of the *in vivo* imaging results, the mice were placed in a cryotome (CM 1950, Leica Microsystems GmbH, Wetzlar, Germany) and imaged using multispectral-cryoslicing imaging using a white light source and a sensitive CCD camera (PCO AG, Donaupark, Kelheim, Germany) as described in Ref. 27. Fluorescence images at the emission wavelength of the probes and white light color images were collected at several cross-sectional positions in the thorax area and employed for comparison with the FMT-XCT images.

3 Results

3.1 Background Fluorescence Calculation and Subtraction

Figure 1 illustrates the steps involved in the calculation of the background fluorescence subtraction.

Figure 1(a) shows the first step in the calculation of the 3-D surface for each projection angle, as described above in methods, at the side of the source S_{source} and the side of the CCD camera S_{CCD} . The calculated distances between the source position \vec{r}_s projected to the source surface S_{source} and all points in the interpolated surface at the side of the CCD camera S_{CCD} constitute the estimate of the normalized background fluorescence IM_{BG} [Fig. 1(b)]. A distribution [Fig. 1(c)] of the calculated background fluorescence image pixels in IM_{BG} divided by the pixels of the acquisition image IM_{acq} [Fig. 1(e)] is calculated as described in methods, showing a peak. We take the peak to correspond with the proportionality factor a , because we assume there is a constant level of background fluorescence throughout the medium, and the peak in the histogram corresponds with the most frequently observed value of $\hat{a}(\vec{r}_d, \vec{r}_s)$ for which $[U^{nB}(\vec{r}_d, \vec{r}_s)]_{measured} = \hat{a}(\vec{r}_d, \vec{r}_s) \|\vec{r}_d - \vec{r}_s\|$. We assume that values higher and lower than this value are due to the fluorescence targets of interest that are also present inside the mouse, or because of in-homogeneities in the optical properties of the tissue.

The second row displays a white light image of the mouse for one projection angle [Fig. 1(d)], an original normalized acquisition image for one source IM_{acq} [Fig. 1(e)] and the corresponding image after fluorescence background subtraction $IM_{corrected}$ [Fig. 1(f)]. It can be understood from the expression derived for the background fluorescence level, which includes the distance from source to detector surface, that areas where the mouse diameter is larger will result in higher levels of background fluorescence in the acquisition image. The image of the calculated background fluorescence level [Fig. 1(b)] reflects this; larger values are calculated for the abdomen, and smaller values are calculated for the sides of the mouse. The same is true for the normalized acquisition image [Fig. 1(e)]. In the background corrected image [Fig. 1(f)], the signal from the abdomen is reduced, and the liver shape is more clearly visible. In the lung area, the level of normalized signal is reduced in general in the corrected image, and small irregularities due to fluorescent targets inside the mouse come to the surface that were not distinguishable in the image before correction.

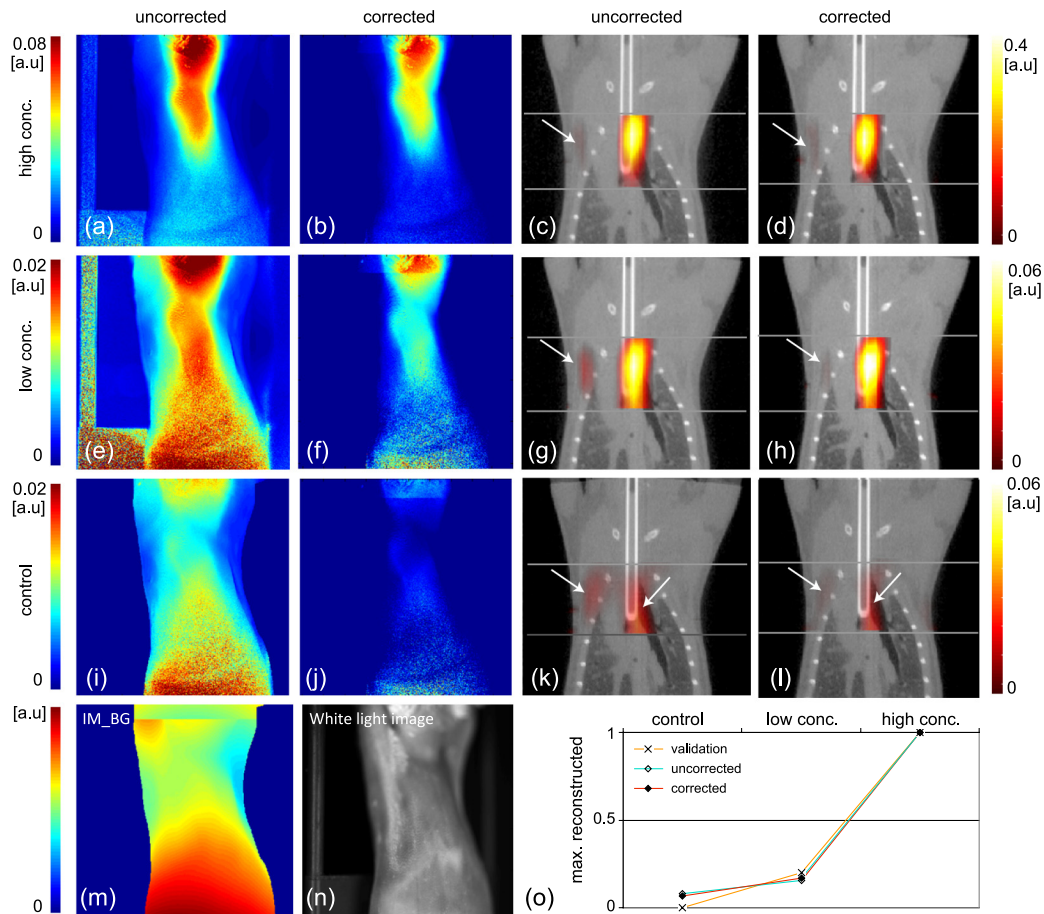


Fig. 2 Effect on quantification: Background correction applied to mouse with tube in esophagus, filled with a mixture containing (a) to (d) fluorochrome in high concentration, conc. 2; (e) to (h) fluorochrome in low concentration, conc. 1; (i) to (l) no fluorochrome. (a), (e), (i) normalized acquisition image for one representative source and projection angle (IM_{acq}); (b), (f), (j) background corrected normalized acquisition data; (c), (g), (k) coronal slice of 3-D FMT-XCT reconstruction intersecting the tube using uncorrected acquisition data; (d), (h), (l) reconstruction using corrected acquisition data; (m) calculated background fluorescence image (IM_{BG}); (n) white light image; (o) graph of max reconstructed values for control and low concentration fluorescence, normalized to high concentration fluorescence (arrows indicate artifacts).

3.2 Effect on Quantification

We evaluated the effect of background fluorescence subtraction on the quantitative properties of FMT-XCT using an *ex vivo* study of a mouse with a tube inserted in the esophagus (Fig. 2). In this case, the background fluorescence arises due to autofluorescence of the tissue only. The tube was filled with a mixture of intralipid, India ink, water, and (1) high concentration fluorochrome protein [Fig. 2(a) to 2(d)]; (2) low-concentration fluorochrome [Fig. 2(e) to 2(h)]; and (3) no fluorochrome (control) [Fig. 2(i) to 2(l)]. Because the same mouse was used for all experiments, and the mouse was not moved during tube insertions, the background fluorescence images [Fig. 2(m)] only needed to be calculated once. The background corrected acquisition images for the two measurements involving a tube filled with a fluorescent mixture [Fig. 2(b) and 2(f)] show a clear indication of the tube, whereas the background corrected acquisition image of the control measurement is almost clear of fluorescence signal [Fig. 2(j)]. The background subtraction has a positive effect on the reconstructed images [Fig. 2(c), 2(g), 2(k), 2(d), 2(h), 2(l)]; before background subtraction, visible artifacts appear in the same place for each of the three cases, which is expected as exactly the same mouse is imaged in exactly the same position, while after background subtraction, the

quantification of the values reconstructed for the tubes is not affected [Fig. 2(o)], but the amount of artifacts due to the background fluorescence is reduced [arrows in Fig. 2(c), 2(g), 2(k), 2(d), 2(h), 2(l)]. The color bar displays signals of low intensity as dark red and signals of high intensity as bright yellow; additionally, we use a linear transparency map that displays signals of low intensity more transparent than signals of high intensity. This way of visualizing the data clearly shows that the number of high-intensity artifacts, which are not affected by the transparency map and could be misinterpreted as target signal, is reduced by using the background subtraction scheme. We quantified the signal in the tube by taking the maximum value. The quantification of the signal in the tube remains the same before and after applying the background subtraction method, demonstrating that the correction method results in reduction of undesired background fluorescence only and that the signal from fluorescent targets present in the mouse is not subtracted.

3.3 In Vivo Study of K-ras Lung Tumor Model

In young, four-week-old K-ras mice, tumor targets were around 0.8 mm, which is close to the maximum resolution that is expected to be achievable with FMT. Not only are the targets

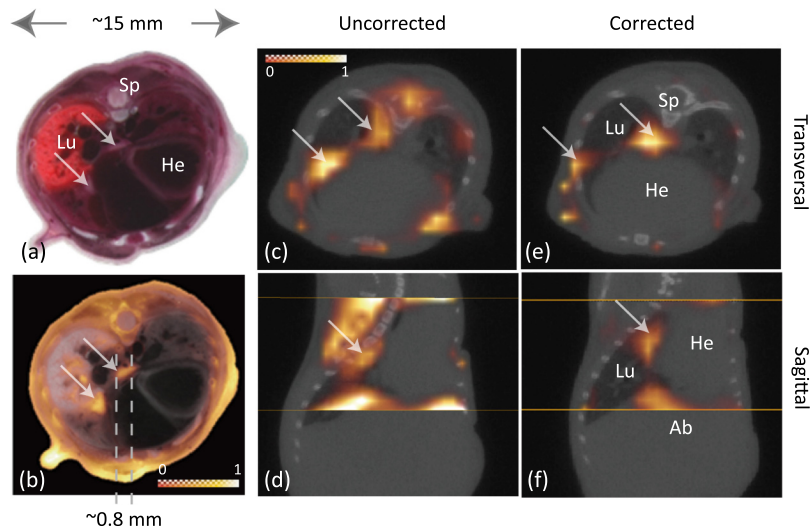


Fig. 3 Hybrid FMT-XCT reconstruction and validation results for four-week-old K-ras: (a) RGB cryoslice image; (b) validation cryoslice showing planar fluorescence in orange; (c), (e) normalized transversal slices and (d) and (f) sagittal slices of FMT-XCT reconstruction based on (c) and (d) uncorrected data and (e) and (f) corrected data (arrows indicate tumors, Sp = Spine, Lu = Lung, He = Heart, Ab = Abdomen, color map displayed in (c) applies to all images, transparency map indicated by checkered pattern).

in young K-ras mice relatively small, the targets are not easily distinguished from the background fluorescence level either. Figure 3(a) and 3(b) shows cryoslicing results for a four-week-old K-ras mouse. The slices are taken from the thorax area of the mouse, displaying the heart and lungs, and two tumors are indicated with arrows. Figure 3(a) shows a white light image, while Fig. 3(b) shows the fluorescence signal in orange overlaid on the white light image reduced to black and white. Background fluorescence is most clearly visible in the tissue surrounding the lung area. Transversal and sagittal slices of the corresponding FMT-XCT reconstructions with and without the background correction applied to the data are displayed in Fig. 3(c) to 3(f). There is a clear reduction in artifacts between the reconstructions based on uncorrected and corrected data for the four-week-old K-ras mouse. The uncorrected reconstruction displays several clear additional fluorescent signals not corresponding with the two small tumors in the lung area, demonstrating the typical effect of background fluorescence not being reconstructed as a homogenous background fluorescence level but as localized artifacts.¹⁸ The resulting corrected reconstruction corresponds well with the validation image [Fig. 3(b)]; it shows two small tumors in the lung in the transversal slice. The coronal slice additionally displays a signal corresponding with the liver area of the mouse. Before applying the background fluorescence correction, it is difficult to distinguish the two small tumors among the reconstructed artifacts, while after applying the background fluorescence correction, the two small tumors can be clearly distinguished from signals of different origin. Also the correspondence of the liver signal with the shape of the liver as seen in the XCT image is improved.

4 Discussion

In this work, we studied the recovery of small objects with hybrid FMT-XCT in the presence of background fluorescence. We exploited the hybrid capabilities of the FMT-XCT system by using the XCT volume for the data-driven calculation of images of the estimated background fluorescence, which we used for preprocessing of the FMT data before reconstruction of the fluorescence bio-distribution.

For the estimation of the background fluorescence, we employed a linear relationship between the 3-D distance from source to detector and the level of background fluorescence, which we assumed to be constant throughout the mouse body. We used the calculated constant together with the XCT volume to estimate normalized images IM_{BG} that would be acquired in case a homogeneous background fluorescence level would be present, which can be subtracted directly from the Born normalized acquisition images IM_{acq} (emission/excitation image). Furthermore, we defined a data-driven estimation method for the calculation of the proportionality constant a , based on the ratio between calculated background fluorescence image and acquired normalized acquisition images for all pixels in a region of interest in the images defined by the area covered by the source positions scanned for the acquisition angle. By performing the background correction directly on the acquisition images, the resolution of the correction is much higher than when it would be done on the source-detector points used in the weight matrix calculation, which is often a reduced representation due to memory restrictions.

Application of the implemented data-driven correction for background fluorescence resulted in improved estimates of the fluorescence bio-distribution *ex vivo* and *in vivo*, characterized by reduction in artifacts attributed to the presence of background fluorescence.

Results of the *ex vivo* mouse study showed that the background correction decreases the amount of artifacts in the reconstruction, while it does not compromise quantification ability; the reconstructed value for the tube stayed the same before and after background correction. We showed that even in mice without an injected fluorescent probe, a low level of background fluorescence can be present and results in undesired artifacts in the reconstruction. Before background correction, these artifacts could be incorrectly interpreted as signal.

In general more varieties of targeted probes (probes that are fluorescent upon injection) exist than varieties of activatable probes (probes that become fluorescent when reaching the site of disease); consequently, targeted probes are being used for most applications. The use of targeted probes inherently results

in a distribution of a low level of background fluorescence throughout the mouse. The constant level of background fluorescence can result in artifacts, which can be misinterpreted as signals.

The ability to distinguish small targets from artifacts arising due to background fluorescence is particularly important when imaging early stage disease progression when targets are smaller and less bright than in later stages. The *in vivo* study of early stage lung cancer displayed that it is possible to reconstruct small targets expressing a low signal compared with the background fluorescence level more accurately after using the correction method. When quantifying the signal strength of fluorescent targets for comparison of disease development in different mice, often relative measures are used that relate the signal in the area of interest to a reference area inside the same mouse; for example, the muscle tissue. Calculation of such a relative measure would be complicated in case the surrounding tissue contains significant artifacts, such as the artifacts visible in the reconstruction of the *in vivo* study before correction. Reduction of artifacts due to background fluorescence is therefore not only important for interpretation of the signal in the area of interest, but also for quantification of the targets relative to other areas of the mouse.

The studies described in this paper show that the algorithm can be used for correcting for a background fluorescence level arising mainly from tissue auto-fluorescence, which was the case in the *ex vivo* study, as well as when the majority of background fluorescence is due to a targeted probe used, as was the case in the *in vivo* study. The assumption is that the background fluorescence level is homogeneous, whether it is auto-fluorescence from the tissue or fluorescence from the probe used will not influence the applicability of the algorithm.

The method and work presented here can be expanded in several directions. In the calculation of the background fluorescence correction, we assumed a homogeneous object with homogeneous optical properties and homogeneous background fluorescence, which allowed us to use a simple calculation for the estimation of the background fluorescence. However, the background fluorescence level can be heterogeneous as well. When imaging the abdomen, for example, large amounts of background fluorescence can be expected from e.g., the liver or the lower intestines, depending on the clearance properties of the probe used and the diet of the mouse. Using the implementation described above, fluorescence originating from distinct structures such as the liver or kidneys will not be removed. This was also demonstrated by the liver signal that is still visible in the reconstruction of the *in vivo* study before and after correction.

A method for subtracting heterogeneous background fluorescence using a second untargeted tracer was successfully developed recently.²³ However, such an approach may not always be feasible, as this requires additional laser and filter sets at the second wavelength, and an untargeted tracer with the same characteristics may not be available; furthermore, it comes with additional cost and additional burden for the animal. The method described in this paper could be extended for cases in which the background fluorescence is inhomogeneous using, for example, the anatomical segmentation of the XCT data for the development of a heterogeneous or layered homogeneous model. After segmentation of the XCT data in anatomical regions based on contrast provided by the use of a CT contrast agent, the expected background fluorescence from these organs

could be calculated and subtracted from the acquisition data before reconstruction by forward modeling their contribution. This can enable imaging of targets that would otherwise be hidden by potentially high background fluorescence levels.

In conclusion, the preprocessing of hybrid FMT-XCT data using the described background fluorescence subtraction method increases the imaging capabilities of hybrid FMT-XCT, leading to a wider range of possibilities for future directions of study.

Acknowledgments

We wish to thank M. W. Koch and A. Sarantopoulos (Institute for Biological and Medical Imaging, Helmholtz Zentrum Munich) for help with FMT-XCT measurements and cryoslicer. VN acknowledges support from EU Framework Program 7 FMT-XCT Grant Agreement No. 201792.

References

1. N. Delioliannis et al., "Free-space fluorescence molecular tomography utilizing 360° geometry projections," *Opt. Lett.* **32**(4), 382–384 (2007).
2. V. Ntziachristos, "Going deeper than microscopy: the optical imaging frontier in biology," *Nat. Methods* **7**(8), 603–614 (2010).
3. F. Leblond et al., "Preclinical whole-body fluorescence imaging: review of instruments, methods and applications," *J. Photochem. Photobiol. B* **98**(1), 77–94 (2010).
4. S. L. Jacques and B. W. Pogue, "Tutorial on diffuse light transport," *J. Biomed. Opt.* **13**(4), 041302 (2008).
5. S. R. Arridge, "Optical tomography in medical imaging," *Inverse Probl.* **15**(2), R41–R93 (1999).
6. R. B. Schulz et al., "Hybrid system for simultaneous fluorescence and x-ray computed tomography," *IEEE Trans. Med. Imaging* **29**(2), 465–473 (2010).
7. V. Ntziachristos, "Optical imaging of molecular signatures in pulmonary inflammation," *Proc. Am. Thorac. Soc.* **6**(5), 416–418 (2009).
8. D. Kephshire et al., "A microcomputed tomography guided fluorescence tomography system for small animal molecular imaging," *Rev. Sci. Instrum.* **80**(4), 043701 (2009).
9. S. C. Davis et al., "Magnetic resonance-coupled fluorescence tomography scanner for molecular imaging of tissue," *Rev. Sci. Instrum.* **79**(6), 064302 (2008).
10. Y. Lin et al., "A gantry-based tri-modality system for bioluminescence tomography," *Rev. Sci. Instrum.* **83**(4), 043708 (2012).
11. D. Hyde et al., "Performance dependence of hybrid x-ray computed tomography/fluorescence molecular tomography on the optical forward problem," *J. Opt. Soc. Am. A Opt. Image Sci. Vis.* **26**(4), 919–923 (2009).
12. T. Pyka et al., "Revisiting the normalized Born approximation: effects of scattering," *Opt. Lett.* **36**(22), 4329–4331 (2011).
13. A. Ale et al., "FMT-XCT: *in vivo* animal studies with hybrid fluorescence molecular tomography-x-ray computed tomography," *Nat. Methods* **9**(6), 615–620 (2012).
14. J. Grimm et al., "Use of gene expression profiling to direct *in vivo* molecular imaging of lung cancer," *Proc. Natl. Acad. Sci. U. S. A.* **102**(40), 14404–14409 (2005).
15. M. J. Nieder et al., "Early photon tomography allows fluorescence detection of lung carcinomas and disease progression in mice *in vivo*," *Proc. Natl. Acad. Sci. U. S. A.* **105**(49), 19126–19131 (2008).
16. J. L. Kovar et al., "A systematic approach to the development of fluorescent contrast agents for optical imaging of mouse cancer models," *Anal. Biochem.* **367**(1), 1–12 (2007).
17. R. Weissleder and V. Ntziachristos, "Shedding light onto live molecular targets," *Nat. Med.* **9**(1), 123–128 (2003).
18. M. Gao et al., "Effects of background fluorescence in fluorescence molecular tomography," *Appl. Opt.* **44**(26), 5468–5474 (2005).
19. J. Chang et al., "Improved reconstruction algorithm for luminescence optical tomography when background lumiphore is present," *Appl. Opt.* **37**(16), 3547–3552 (1998).

20. N. Deliolanis et al., "In vivo tomographic imaging of red-shifted fluorescent proteins," *Biomed. Opt. Express* **2**(4), 887–900 (2011).
21. A. Soubret and V. Ntziachristos, "Fluorescence molecular tomography in the presence of background fluorescence," *Phys. Med. Biol.* **51**(16), 3983–4001 (2006).
22. R. M. Levenson et al., "Multiplexing with multispectral imaging: from mice to microscopy," *ILAR J.* **49**(1), 78–88 (2008).
23. K. M. Tichauer et al., "Dual-tracer background subtraction approach for fluorescent molecular tomography," *J. Biomed. Opt.* **18**(1), 016003 (2013).
24. J. R. Mansfield et al., "Autofluorescence removal, multiplexing, and automated analysis methods for in vivo fluorescence imaging," *J. Biomed. Opt.* **10**(4), 041207 (2005).
25. K. Radrich et al., "Improving limited-projection-angle fluorescence molecular tomography using a co-registered x-ray computed tomography scan," *J. Biomed. Opt.* **17**(12), 126011 (2012).
26. L. Johnson et al., "Somatic activation of the K-ras oncogene causes early onset lung cancer in mice," *Nature* **410**(6832), 1111–1116 (2001).
27. A. Sarantopoulos, G. Themelis, and V. Ntziachristos, "Imaging the bio-distribution of fluorescent probes using multispectral epi-illumination cryoslicing imaging," *Mol. Imaging Biol.* **13**(5), 874–885 (2011).